

SparseVLR: A Novel Framework for Verified Locally Robust Sparse Neural Networks Search

Sawinder Kaur
 Department of EECS
 Syracuse University
 sakaur@syr.edu

Asif Salekin
 Department of EECS
 Syracuse University
 asalekin@syr.edu

Abstract

The compute-intensive nature of neural networks (NNs) limits their deployment in resource-constrained environments such as cell phones, drones, autonomous robots, etc. Hence, developing robust sparse models fit for safety-critical applications has been an issue of longstanding interest. Though adversarial training with model sparsification has been combined to attain the goal, conventional adversarial training approaches provide no formal guarantee that the models would be robust against any rogue samples in a restricted space around a benign sample. Recently proposed verified local robustness techniques provide such a guarantee. This is the first paper that combines the ideas from verified local robustness and dynamic sparse training to develop ‘SparseVLR’— a novel framework to search verified locally robust sparse networks. Obtained sparse models exhibit accuracy and robustness comparable to their dense counterparts at sparsity as high as 99%. Furthermore, unlike most conventional sparsification techniques, SparseVLR does not require a pre-trained dense model, reducing the training time by 50%. We exhaustively investigated SparseVLR’s efficacy and generalizability by evaluating various benchmark and application-specific datasets across several models.

1 Introduction

The application of neural networks (NNs) in safety-critical systems requires a framework for formal guarantees regarding their functioning [23]. The brittle nature of NNs renders them vulnerable to imperceptible adversarial perturbation ε , which can lead to inaccurate model prediction [13], and the actions triggered based on these incorrect predictions may have catastrophic effects [35].

The empirical adversarial training for NN models relies on efficiently finding adversarial perturbations around individual samples leveraging existing adversarial attacks. However, such training cannot guarantee that no other (yet

unknown) attacks would find adversarial samples in the ℓ_p -ball of radius ε around the respective samples [61].

For instance, Madry *et al.* [31] used the PGD attack to generate worst-case perturbations to be used for adversarial training. Recent approaches [38, 52, 62] have proposed several mechanisms to improve upon the baseline adversarial training mechanism [31], but to generate adversarial samples for training, these approaches employ PGD attack of varying strengths. However, Tjeng *et al.* [50] showed that PGD does not necessarily generate the perturbations with maximum loss; thus, the models trained to minimize PGD adversarial loss were still vulnerable to other stronger attacks. On the contrary, verified local robustness training [14, 23, 56, 60] guarantees the non-existence of adversarial samples in the vicinity of the benign samples, making it essential for safety-critical systems.

Model Compression - A Necessity. The enormous number of parameters present in dense NNs challenge their deployment in resource-constrained environments such as self-navigation, hazard detection, etc., making it essential to generate sparser NN models. The majority of the existing works that focus on obtaining sparse NN models aim to maintain the prediction (benign) accuracy of the sparse model comparable to the dense models trained with the same objective [1, 16, 17, 25, 39, 40, 63]. Recently, works are aiming at the additional target of adversarial robustness for a certain attack alongside benign accuracy [24, 44, 45]. This first-of-its-kind work extends the scope to obtaining sparse NN networks which exhibit high accuracy and verified local robustness (definition is provided in Sec. 2.2) while using significantly fewer parameters (1% of the comparable verified locally robust dense networks evaluated in literature).

Pruning is the most common form of sparsification mechanism used in literature [16, 17, 25, 40, 44, 45, 63]. Our preliminary study (Sec. 3) leveraging pruning mechanisms establishes the existence of verified locally robust sparse networks as sub-networks of dense verified locally robust models. Though conventional pruning fails, pruning combined with Dynamic Sparse Training (DST) [4] can achieve

such sparse networks comparable in generalizability to their denser counterparts. In this work, we referred to *model generalizability* as the ability of the model to project high (benign) accuracy and verified local robustness simultaneously.

However, pruning requires a fully converged dense NN to start with, which is computationally expensive. Above mentioned findings motivate *this study to adapt DST to achieve locally robust sparse networks from scratch* without such a requirement. Notably, this paper’s empirical evaluations show that obtaining a sparse network from scratch results in even higher generalizability and sparsity.

In summary, the contributions of the paper are:

1. This *first-of-its-kind* work presents **SparseVLR**— an approach to train a sparse locally robust model without training a dense over-parameterized model (Sec. 4). The sparse models exhibit similar generalizability but utilize significantly (up to 1%) fewer parameters than their denser counterparts evaluated in the literature.
2. This paper performs a detailed empirical analysis to understand the high effectiveness of **SparseVLR** (Sec. 5.1). It identifies that the DST and using randomly initialized sparse network as the starting network, results in high gradient flow during training, allowing the model to learn new concepts by exploring new network connections.
3. Our empirical study (Sec. 5) demonstrates that **SparseVLR** is effective on benchmark image datasets (MNIST and CIFAR-10) and model architecture combinations used in the literature, as well as on application-relevant datasets: SVHN, *Pedestrian Detection* [33], and sentiment analysis NLP dataset [30].

Additionally, Sec. 2 provides relevant backgrounds and related work discussion, Sec. 6 presents evaluations on some design choices of **SparseVLR**, and Sec. 7 discusses the impact, limitations and future-work scope of this study. Notably, our comprehensive Appendix further discusses the datasets, hyper-parameters, seeds, models, backgrounds, and detailed analysis of different aspects of **SparseVLR**.

2 Background and Related-Works

2.1 Formal Robustness Verification

Formal robustness verification of non-linear NNs is an NP-complete problem (discussed in Appendix B). Recent Linear Relaxation based Perturbation Analysis (LiRPA) methods can verify non-linear NNs in polynomial time. These methods use Forward (IBP [14]), Backward (CROWN [61], Fastened-CROWN [29], α -CROWN [57], β -CROWN [51], DeepPoly [46], BaB Attack [58]) or Hybrid (CROWN-IBP [60]) bounding mechanisms to compute linear relaxation of a model.

Specifically, for each sample x_0 , the perturbation neighborhood is defined as ℓ_p -ball of radius ε as

$$\mathbb{B}_p(x_0, \varepsilon) := \{x \mid \|x - x_0\|_p \leq \varepsilon\}. \quad (1)$$

LiRPA aims to compute linear approximations f^ε of the model \mathcal{M}_θ (θ represents model parameters), and provide lower f_L^ε and upper f_U^ε bounds at the output layer, such that for any sample $x \in \mathbb{B}_p(x_0, \varepsilon)$ and each class j , the model output is guaranteed to follow:

$$f_L^\varepsilon(x)^j \leq \mathcal{M}_\theta(x)^j \leq f_U^\varepsilon(x)^j. \quad (2)$$

2.2 Verified Local Robustness.

A NN model, \mathcal{M}_θ is said to be verified locally robust [10] for a sample (x_0, y) if: $\forall x \in \mathbb{B}_p(x_0, \varepsilon) \Rightarrow \mathcal{M}_\theta(x) = \mathcal{M}_\theta(x_0)$, scilicet for all the samples $x \in \mathbb{B}_p(x_0, \varepsilon)$, the model is guaranteed to assign the same class as it assigns to x_0 . LiRPA approaches measure the local robustness in terms of a margin vector $m(x_0, \varepsilon) = Cf^\varepsilon(x_0)$, where C is a *specification matrix* of size $n \times n$ and n is the number of all possible classes [14, 56, 60, 61]. Zhang *et al.* [60] defines C for each sample (x_0, y) as:

$$C_{i,j} = \begin{cases} 1, & j = y \text{ and } i \neq y \text{ (truth class)} \\ -1, & i = j \text{ and } i \neq y \text{ (other classes)} \\ 0, & \text{otherwise.} \end{cases} \quad (3)$$

The entries in matrix C depend on the true class y . In matrix C , the row corresponding to the true class contains 0 at all the indices. All the other rows, contain 1 at index corresponding to the true class ($j = y$) and -1 at index corresponding to current class ($j = i$) and 0 at all the other indices. Thus, the i^{th} value of $m(x_0, \varepsilon)$ is given by $m^i(x_0, \varepsilon) = f^\varepsilon(x_0)^y - f^\varepsilon(x_0)^i$, which is the difference of output values of the true class y with all the other classes.

$m(x_0, \varepsilon)$ represents the lower bound of the margin vector. If all the values of the $m(x_0, \varepsilon)$ are positive, $\forall_{i \neq y} m^i(x_0, \varepsilon) > 0$, the model \mathcal{M}_θ is said to be locally robust for sample x_0 . That implies, the model will always assign the highest output value to the true class label y if a perturbation less than or equal to ε is induced to the sample x_0 . Thus, $\forall_j m(x_0, \varepsilon)^j > 0$ implies the guaranteed absence of any adversarial sample in the region of interest. Furthermore, to specify the region bounded by $\mathbb{B}_p(x_0, \varepsilon)$, we use $p = \infty$ because ℓ_∞ -norm covers the largest region [53].

2.3 Model Training to Maximize Local Robustness

Since, a model is considered verified locally robust for a sample (x_0, y) if all the values of $m(x_0, \varepsilon) > 0$, the training schemes proposed by previous approaches [14, 60] aim to

maximize robustness of a model by maximizing the lower bound $\underline{m}(x_0, \varepsilon)$. Xu *et al.* [56] defines the training objective as minimizing the maximum cross-entropy loss between the model output $\mathcal{M}_\theta(x)$ and the true label y among all samples $x \in \mathbb{B}_p(x_0, \varepsilon)$ (eq. 6 in [56]). Thus,

$$\mathcal{L}_{\text{train}}(\mathcal{M}_\theta, \mathcal{D}, \varepsilon) = \sum_{(x_0, y) \in \mathcal{D}} \max_{x \in \mathbb{B}(x_0, \varepsilon)} \mathcal{L}(\mathcal{M}_\theta(x), y), \quad (4)$$

where \mathcal{D} is the dataset and $(x_0, y) \in \mathcal{D}$. Intuitively, $\mathcal{L}_{\text{train}}$ is the sum of maximum cross-entropy loss in the neighborhood of each sample in \mathcal{D} for perturbation amount ε . Wong and Kolter [54] showed that the problem of minimizing $\mathcal{L}_{\text{train}}$ (as defined in Eq. (4)) and the problem of maximizing $\underline{m}(x_0, \varepsilon)$ are dual of each other. Thus, *a solution that minimizes $\mathcal{L}_{\text{train}}$, maximizes the values of $\underline{m}(x_0, \varepsilon)$, hence maximizes the local robustness for the sample (x_0, y) .* Since, $x_0 \in \mathbb{B}_p(x_0, \varepsilon)$, *minimizing $\mathcal{L}_{\text{train}}$ also maximizes benign accuracy, ergo maximizes generalizability altogether.*

Xu *et al.* [56] computes $\max_{x \in \mathbb{B}(x_0, \varepsilon)} \mathcal{L}(\mathcal{M}_\theta(x), y)$ which requires computing bounding planes f_U^ε and f_L^ε using one of the aforementioned LiRPA bounding techniques. Following Xu *et al.* [56], **SparseVLR** employs CROWN-IBP hybrid approach as the bounding mechanism to optimize $\mathcal{L}_{\text{train}}(\mathcal{M}_\theta, \mathcal{D}, \varepsilon)$ in Eq. (4). The perturbation amount ε is initially set to zero and gradually increases to ε_{max} according to the perturbation scheduler ε -scheduler($\varepsilon_{\text{max}}, t, s, l$) discussed in Appendix B.1.

Metrics for evaluations: Tab. 1 defines the metrics used to evaluate models which have been used in the previous works for formal robustness verification [14, 56, 60, 61].

Error	Definition
Standard	% of benign samples classified incorrectly.
Verified	% of benign samples for which at least one value in the $\underline{m}(x_0, \varepsilon)$ is negative.
PGD	% of perturbed samples, generated using 200-step PGD attack, classified incorrectly.

Table 1. Evaluation metrics. Here, % implies percentage.

2.4 Model Sparsification

Model Sparsification is the most common form of model compression, which constrains the model to use only a subset of model parameters for inference [16, 17, 25, 40, 44, 45, 63]. Hoefler *et al.* [19] categorizes the model sparsification based on the stage at which sparsification is performed: • *train-and-sparsify*: pruning a fully trained model often followed by re-training (finetuning) the retained parameters [16, 44, 45, 63], • *sparsifying-during-training*: multiple rounds of *train-and-sparsify* while increasing sparsity in every round a.k.a. iterative pruning [49, 59] and • *sparse-training*: training a sparse network using either a static [7–9, 32, 42] or dynamic [4, 26] mask.

Recently developed *dynamic-mask-based sparse-training* known as Dynamic Sparse Training (DST) [4, 26] approaches iteratively follow *grow-and-prune* paradigm to achieve an optimal sparse network. Starting from a random sparse *seed network*, new connections (i.e., parameters) which minimize the natural loss are added (*grow step*), and the least important connections are removed (*prune step*). DST’s higher efficacy than the *static-mask-based sparse-training* is attributed to high gradient flow allowing the model to learn an optimal sparse network for effective inference generation [6]. **SparseVLR** adapts the DST approach to identify and train verified locally robust sparse networks from scratch.

Parameter removal or pruning: **SparseVLR** uses global magnitude-based pruning, an unstructured pruning mechanism [37], as multiple works [11, 27, 28, 43, 47] suggest its higher efficacy in achieving more generalizable sparse networks. It also captures the importance of a layer as a whole [41]. Additionally, magnitude-based pruning approaches [15–17, 25, 40, 44, 45, 63] remove the least magnitude parameters suggesting that the importance of a parameter is directly proportional to the magnitude of its weights.

There is rich literature on sparsification mechanisms and parameter removal. A detailed summary is in Appendix C.

3 Motivation: Existence of Verified Locally Robust Sparse Network

Zhang *et al.* [60] noted that the verified local robustness training mechanism proposed by Wong and Kolter [54] and Wong *et al.* [55] induce an implicit regularization, thus, penalizing the magnitude of model parameters during training. CROWN-IBP [60] training incurs less regularization and shows an increasing trend in the magnitude of model parameters while training. According to our preliminary analysis discussed in Appendix D, the implicit regularization caused by CROWN-IBP does penalize networks’ parameters, making them smaller as compared to naturally trained networks, causing a high fraction of the parameters to be close to zero (magnitude $\approx 10^{-40}$). Removal of such less significant parameters has minimal impact on model generalizability, which indicates *the existence of a sparse sub-network that exhibits verified local robustness comparable to its dense counterpart*.

Fig. 1 demonstrates the *standard* and *verified* errors for 4-layer CNN trained to minimize L_{train} defined in Eq. (4) for benchmark datasets MNIST and CIFAR-10 at various compression amounts. The evaluations are shown for the (i) Global Pruning without any finetuning or re-training, (ii) Conventionally finetuning a globally pruned network using a static mask, and (iii) Re-training the pruned network using DST-based *grow-and-prune* technique [4].

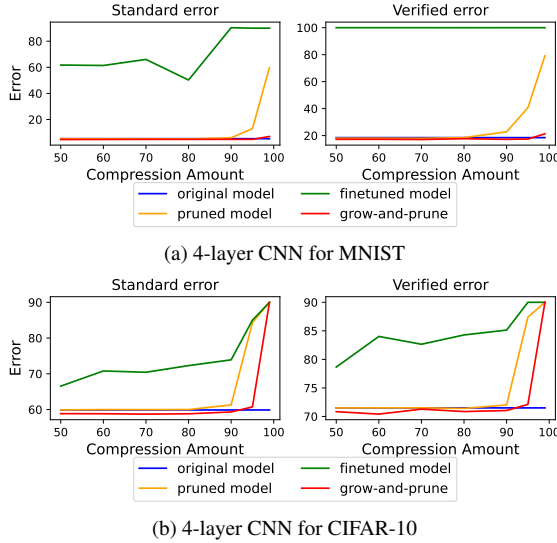


Figure 1. Accuracy and local robustness of dense model (original model) vs pruned model at different pruning amounts obtained using (i) global pruning (pruned model), (ii) global pruning followed by fine-tuning (finetuned model), and (iii) re-training using grow-and-prune (grow and prune) for 4-layer CNN for (a) MNIST ($\varepsilon = 0.4$) and (b) CIFAR-10 ($\varepsilon = 8/255$)

Fig. 1 shows that as the compression ratio increases ($> 90\%$), weights having higher significance on model inference become the pruning target. Thus, the model generalization, in terms of natural accuracy and robustness, drops significantly, resulting in a *trivial classifier*¹ in extreme cases. Conventional finetuning (#ii) increases the *standard* and *verified* error even at small compression amounts. However, re-training using *grow-and-prune* (#iii) maintains the generalizability of the sparse models at relatively high compression amounts. A comparison of (#i) & (#iii) for 7-layer CNN and Resnet is provided in Appendix E.

The effectiveness of *grow-and-prune* (#iii) in re-training a pruned model can be attributed to the better gradient flow encountered during training as compared to conventional static-mask-based finetuning (#ii), which is in agreement with [6]. A discussion of their gradient flow and loss evolution during training is provided in Appendix E.

Moreover, according to our preliminary analysis, locally robust sparse training leveraging static-mask-based sparsifying-during-training approaches such as *iterative pruning* [49] results in inferior performance.

This section establishes (1) the existence of verified locally robust sparse sub-network in dense verified robustly trained models; and (2) *grow-and-prune* training paradigm can help identify such sparse networks.

¹A classifier that always predicts the same class irrespective of the input

Algorithm 1 SparseVLR

Require: \mathcal{M}_θ : Backbone architecture $\diamond p$: Target sparsity $\in (0, 100)$ $\diamond \mathcal{D} = (X_i, y_i)_{i=1}^m$: Dataset $\diamond \varepsilon_{\max}$: Maximum Perturbation $\diamond T$: Number of training epochs $\diamond (s, l)$: Start and length of perturbation scheduler $\diamond \text{seed}$: A seed value

- 1: Randomly initialize the backbone architecture using *seed*.
- 2: $\theta^\downarrow = [m | m \in p^{\text{th}} \text{ percentile of } |\theta|]$ \triangleright Select the highest $(100-p)\%$ parameters of \mathcal{M}_θ to form a sparse seed network $\mathcal{M}_{\theta^\downarrow}$ while making remaining parameters dormant.
- 3: **for** epoch $t = [0, 1, \dots, T]$ **do**
- 4: $\varepsilon_t = \varepsilon\text{-Scheduler}(\varepsilon_{\max}, t, s, l)$
- 5: **for** minibatches $d \in \mathcal{D}$ **do**
- 6: $\mathcal{M}_{\theta^\downarrow} = \underset{\theta}{\operatorname{argmin}} \mathcal{L}_{\text{train}}(\mathcal{M}_{\theta^\downarrow}, d, \varepsilon_t)$ \triangleright Auxiliary Model $\mathcal{M}_{\theta^\downarrow}$ is denser than target sparsity, i.e. $|\theta'| > |\theta^\downarrow|$
- 7: **end for**
- 8: $\theta^\downarrow = [m | m \in p^{\text{th}} \text{ percentile of } |\theta|]$ \triangleright Select the highest $(100-p)\%$ parameters of \mathcal{M}_θ , ergo the highest k' parameters of $\mathcal{M}_{\theta^\downarrow}$ to obtain target sparsity
- 9: **end for**

4 Verified Locally Robust Sparse Model via Dynamic-Mask-based Sparse-training

Motivated by the above-discussed findings, this paper presents a dynamic-mask-based sparse-training mechanism to achieve a verified locally robust sparse network without training a dense over-parameterized model. **SparseVLR** is based on *grow-and-prune* paradigm [4], which allows network connections to expand under the constraints of an underlying backbone architecture. Each parameter of the backbone model can either be in *active* or *dormant* state based on whether or not it belongs to the sparse network at a particular instant. The weight of a *dormant* parameter is set to zero. The percentage of parameters that are *dormant* is the network's current *sparsity*.

4.1 Problem Definition:

For a given randomly initialized backbone architecture \mathcal{M}_θ with k parameters, the objective is to train a verified locally robust sparse network $\mathcal{M}_{\theta^\downarrow}$ which uses only a subset of available parameters (of the backbone), that is, $|\theta^\downarrow|_0 = k'$ and k' is an order of magnitude times smaller than k , $k' \ll k$. The sparse model thus achieved should exhibit high accuracy and verified local robustness, comparable to a verified locally robust dense network having the same backbone architecture.

4.2 SparseVLR: The Approach

Algorithm 1 describes the **SparseVLR** procedure. It requires a backbone architecture M_θ ; a target sparsity p , the dataset \mathcal{D} ; and the maximum perturbation ε_{\max} . It also requires hyperparameters that vary for different datasets and includes the number of training epochs T and the inputs for the ε -scheduler: s and l (discussed in Appendix A).

SparseVLR starts with an untrained random sparse (i.e., seed) network while keeping $p\%$ parameters of the backbone as dormant ($p = (1 - \frac{k}{k}) \times 100$). It is an iterative procedure, and each iteration comprises two phases: • *Thickening*: aims to explore new parameters in the backbone to maximize verified local robustness resulting in lesser sparsity, and • *Pruning*: removes parameters that hold lesser importance for model inference to reach the target sparsity at the end of each iteration.

Seed Network (lines 1-2 in Algorithm 1) Given a backbone architecture, a sparse seed network is computed by randomly initializing all the backbone parameters, followed by retaining the parameters having only the top $(100 - p)\%$ weight magnitudes. All the other parameters of the backbone are set to zero (made dormant).

Thickening (lines 4-7 in Algorithm 1) This phase aims to densify the sparse network by inspecting all possible parameters (within the backbone). The parameter weights, including the *dormant* ones, are updated according to their corresponding gradients. This is also referred to as *gradient based growth phase* in the literature [4, 6, 26]. However, in literature, gradients are computed for the objective of maximizing benign accuracy, that is, minimizing the *standard* error; in contrast, **SparseVLR** aims to maximize verified local robustness of the model by minimizing the training loss $\mathcal{L}_{\text{train}}$ as defined in Eq. (4) for each mini-batch $d \in \mathcal{D}$. The perturbation ε used for computing $\mathcal{L}_{\text{train}}$ is computed using the perturbation scheduler ε -scheduler($\varepsilon_{\max}, t, s, l$) as discussed in Appendix B.1.

The updated network $M_{\theta'}$ is called *auxiliary network*. Since there is no restriction on the capacity of the *auxiliary network*, it can have more than k' active parameters.

Pruning (line 8 in Algorithm 1) The auxiliary network obtained after the *Thickening* phase needs to be compressed to the target size k' . This phase aims to reduce the model size in terms of the number of *active* parameters while having minimum impact on the generalizability. As discussed in Sec. 2, to be consistent with the state-of-the-art, we employ ℓ_1 -unstructured global pruning as the model sparsification mechanism [34], to attain the sparse network $M_{\theta'}$ with target size k' . Our sparsification uses ℓ_1 -norm of individual model parameters as the metric to decide its importance towards model inference. Notably, ℓ_1 -norm corresponds to the magnitude of the weight of the individual parameters.

However, Liu *et al.* [27] also showed that global pruning could result in a disconnected network. This can be prob-

lematic for the approaches which use single-shot pruning, that is, pruning a fully trained network followed by finetuning only the retained parameters. **SparseVLR** dynamically explores and selects the connections which minimize the training loss, thus, eliminating the chances of receiving a disconnected network.

5 Experiments

This section empirically demonstrates: **1)** The effectiveness of **SparseVLR** in achieving verified locally robust sparse models (Sec. 5.1). **(2)** The dynamic masking used by **SparseVLR** results in high gradient flow (Sec. 5.1(i)-(ii)), which allows the model to learn new concepts (Sec. 5.1(iii)), which aligns with the finding of [6]. **(3)** Inheriting the weight initialization from a fully converged dense model to obtain a sparse model result in ineffective training at high sparsity (Sec. 5.1(iv)). Moreover, **(4)** the generalizability of **SparseVLR** is demonstrated by evaluating sequential networks (i.e., LSTM), and **(5)** finally, an evaluation is shown for practical application relevant datasets: SVHN (Street View House Numbers), Pedestrian Detection [33], and NLP dataset for sentiment analysis [30].

Datasets and Models: To establish the empirical effectiveness of **SparseVLR**, we use benchmark datasets MNIST and CIFAR-10, which are used in the previous works [14, 54–56, 60, 61]. To demonstrate the versatility of the approach across different architectures, we evaluate (a) Two CNNs with varying capacity: 4-layer CNN and 7-layer CNN [14, 60]; (b) Network with skip connections: A 13-layer ResNet used by [55] (c) A sequential network: LSTM used by [56]. To demonstrate the effectiveness and generalizability of **SparseVLR**, evaluations are shown for application-relevant datasets: SVHN, Pedestrian Detection [33], and Sentiment Analysis [30]. Further details about perturbations and hyperparameters are discussed in Appendix A.

Formal Verification Mechanisms to compute $\mathcal{L}_{\text{train}}$ and *verified error*: While training a sparse network, **SparseVLR** employs CROWN-IBP [60]. In Sec. 6, we show empirically that the sparse models trained using CROWN-IBP exhibit lower errors than sparse models obtained using other bounding mechanisms such as IBP [14], CROWN [61], and Fastened-CROWN [29]. For evaluations, to be consistent with the state-of-the-art [14, 56, 60], the presented evaluations use IBP to compute *verified error*.

Nomenclature & abbreviations for the Evaluated Sparse Networks: We aim to train an optimal sparse network that exhibits high accuracy and verified robustness starting from a random sparse network as the seed. However, conventional pruning approaches generally require a fully converged dense network as the starting point.

Dataset			MNIST				CIFAR-10			
Model	$\mathcal{M}_{\theta \downarrow}$ Type	Sparsity \Rightarrow \mathcal{M}_{θ}	0%	90%	95%	99%	0%	90%	95%	99%
			Error							
4-layer CNN	PM^T	Standard	5.29	4.79	4.78	6.97	59.88	59.32	60.73	90.0
		PGD	10.93	6.30	6.23	8.98	67.25	66.01	66.74	90.90
		Verified	18.07	17.22	17.46	21.35	71.5	71.04	72.12	90.0
	RSM^T	Standard		5.71	6.59	8.09		60.78	61.26	64.14
		PGD		7.62	9.00	10.63		67.08	67.13	69.09
		Verified		19.33	20.84	23.14		71.90	72.45	73.43
7-layer CNN	PM^T	Standard	2.27	2.05	3.37	2.11	56.08	55.33	55.24	90.0
		PGD	6.19	3.93	4.85	3.61	68.65	67.59	67.21	90.0
		Verified	12.2	11.96	14.51	12.06	68.66	68.49	69.6	90.0
	RSM^T	Standard		2.32	3.01	2.76		55.41	56.96	59.14
		PGD		3.88	4.21	4.75		68.26	68.30	67.04
		Verified		12.39	12.6	12.83		68.84	69.12	71.21
Resnet	PM^T	Standard	3.65	3.23	3.17	3.12	53.6	55.17	90.0	90.0
		PGD	9.11	4.16	4.04	3.98	63.83	66.25	90.0	90.0
		Verified	14.30	13.52	13.34	13.80	68.58	69.28	90.0	90.0
	RSM^T	Standard		3.91	3.88	4.95		56.30	57.99	60.31
		PGD		5.05	5.16	6.77		67.44	67.04	68.88
		Verified		15.06	15.39	17.74		69.33	70.14	71.38

Table 2. Error Metrics for 4-layer CNN, 7-layer CNN and Resnet trained for MNIST ($\varepsilon_{\text{train}} = 0.4$ and $\varepsilon_{\text{test}} = 0.4$) and CIFAR ($\varepsilon_{\text{train}} = 8.8/255$ and $\varepsilon_{\text{test}} = 8/255$) at different sparsity amounts

To compare, this section evaluates *thickening-and-pruning*-based sparse model training (lines 3-9 of Algorithm 1) using two different starting/seed sparse network variations:

- Random Sparse Model (RSM): This is the seed network used in **SparseVLR** in Sec. 4.2 and is obtained by applying global magnitude-based pruning to the randomly initialized backbone architecture.
- Pruned Model (PM): PM is the same as (#i) model in Sec. 3, obtained by applying global magnitude-based pruning to a fully converged dense model.

The final models obtained after applying Algorithm 1 (lines 3-9) to PM and RSM are denoted by PM^T and RSM^T . PM^T is similar to the (#iii) in Sec. 3.

5.1 Establishing the Effectiveness of **SparseVLR**:

Tab. 2 shows the results for empirical analysis of **SparseVLR** for the benchmark datasets MNIST and CIFAR10. The results are shown for three models: 4-layer CNN, 7-layer CNN, and Resnet at sparsity amounts 90%, 95%, and 99%. The models are evaluated through *standard*, *PGD*, and *Verified* errors as described in Sec. 2. The column corresponding to 0% sparsity represents the error metrics computed for dense models (having the same architecture as the backbone in Algorithm 1) trained using Xu *et al.* [56], which aligns well with the state-of-the-art [55,60]. The presented results are averaged over five random initializations (seeds) on Algorithm 1.

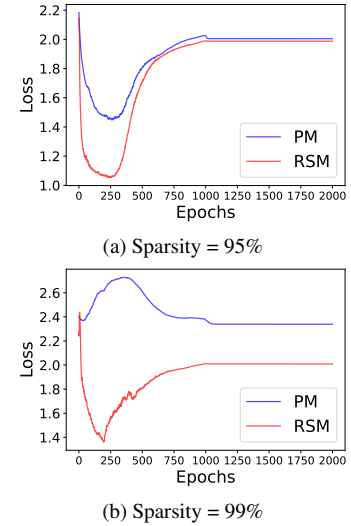


Figure 3. Variation of training loss for CIFAR-10 dataset on 4-layer CNN with $\varepsilon_{\text{test}} = 8/255$ at two sparsity amounts (a) 95% and (b) 99%

According to the Tab. 2, RSM^T achieves similar evaluation metrics (within 3% verified error) as the dense (0% sparsity) models across all datasets, models, and sparsity amounts. *These results establish that (i) **SparseVLR** can train a verified locally robust sparse model without needing a dense over-parameterized network trained till convergence, and (ii) The sparse model thus obtained is comparable to the verified locally robust dense network with the same architecture as the backbone.*

Also, RSM^T outperforms PM^T (the best approach from Sec. 3). Tab. 2 shows that across all model-dataset scenarios, the error metrics for RSM^T are comparable to PM^T at smaller sparsity and at higher sparsity (e.g., 99%) RSM^T exhibits much less error than PM^T , establishing **SparseVLR**'s (Algorithm 1) higher efficacy compared to the conventional pruning mechanisms. Comparisons for PM, PM^T , and RSM^T are provided in Appendix E.

To investigate the reason for the better performance of **SparseVLR**, a detailed analysis for 4-layer CNN trained for CIFAR-10 is provided; however, similar patterns were observed for other models as well.

(i) Why the RSM^T vs. PM^T disparity at higher sparsity?

Fig. 3(a) depicts the loss evolution for $\text{PM} \rightarrow \text{PM}^T$ and $\text{RSM} \rightarrow \text{RSM}^T$ training at 95% sparsity, and reveals that the losses eventually stabilize at the same level, which in turn is governed by the maximum perturbation ε_{max} . **SparseVLR** uses ε -scheduling, which provides 0 perturbation for initial s epochs and then gradually increases the perturbation value. This results in an initial drop in losses, as seen in figures Fig. 3(a). As the perturbation amount increases, the

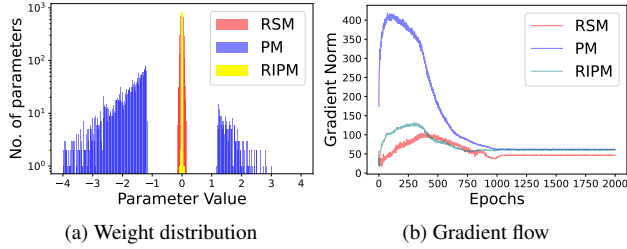


Figure 4. (a) Distribution of weights and (b) Gradient flow encounters while training RSM, PM and RIPM for a 4-layer CNN for CIFAR-10 dataset at 99% sparsity

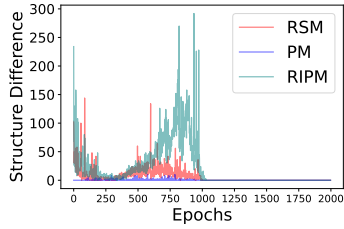


Figure 5. Changes in sparse model structure while training a 4-layer CNN for CIFAR-10 dataset $\varepsilon_{\text{train}} = 8.8/255$ at 99% sparsity using RSM, PM and RIPM as seed networks

loss increases as well.

Notably, at 99% sparsity (Fig. 3(b)), the stabilized loss for PM^T is significantly greater than RSM^T . Higher loss leads to higher error, hence, the observation. The evolution of training loss of PM^T is discussed further in Appendix E. The reason for the higher stabilized loss for PM^T at high sparsity is discussed below.

(ii) Reason for disparity in the stabilized losses for RSM^T and PM^T : Gradient flow over $\mathcal{L}_{\text{train}}$

Evci *et al.* [6] claims that different initialization may lead to different gradient flow, which in turn leads to varied accuracy of the sparse model trained via DST. To explain the disparity in stabilized losses for PM^T and RSM^T at 99% sparsity (Fig. 3b), we plot the observed gradient flows in Fig. 4(b). It depicts that the ℓ_1 -norm of gradients observed while training $\text{RSM} \rightarrow \text{RSM}^T$ is greater than the gradient norm incurred while training $\text{PM} \rightarrow \text{PM}^T$, thus, allowing the model to learn new concepts (further discussed below), hence incurring a lower stabilized loss.

(iii) How poor gradient flow hinders the ability of the sparse network to change connections (i.e., learning new concepts) during training?

The effect of poor gradient flows is two-fold: (i) a lesser number of parameters explored (activated) during the thickening phase, and (ii) relatively small magnitude in the newly activated parameters of the auxiliary model.

The change in the structure of a sparse network obtained after a pruning step can be quantified in terms of the number of parameters of the backbone whose state changed

from active to dormant and vice-versa. Fig. 5 depicts the changes in the sparse structure during training. Notably, $\text{PM} \rightarrow \text{PM}^T$ training incurs almost no change, whereas the sparse structure of $\text{RSM} \rightarrow \text{RSM}^T$ training is quite dynamic. This can be attributed to smaller magnitudes of newly activated parameters which become an easy target of removal during the pruning step, resulting in a similar sparse structure. It further hinders the sparse network's ability to learn new concepts, leading to a higher loss in PM^T than RSM^T .

(iv) Cause for inefficient learning while training $\text{PM} \rightarrow \text{PM}^T$ - Is it the structure or the weight initialization?

PM inherits parameter weights from a pre-trained dense model, and the PM structure is learned through global magnitude-based pruning. This section investigates whether the lower performance of PM^T at high sparsity (e.g., 99%) is due to PM 's retained parameter weights or learned network structure.

For this investigation, we evaluate the Randomly Initialized Pruned Model (RIPM) as the seed network, which randomly initializes PM 's parameters while keeping the learned structure intact. Tab. 3 compares RIPM^T , the sparse model obtained via training $\text{RIPM} \rightarrow \text{RIPM}^T$ using Algorithm 1 (lines 3 – 9), with PM , PM^T , and RSM^T . It can be observed that RIPM^T generalizes comparable to RSM^T . Also, Fig. 5 suggests that while training $\text{RIPM} \rightarrow \text{RIPM}^T$, the model can learn new connections (high variation in the sparse network structure) in the first half of training.

However, Fig. 4(b) shows that the gradient flow while training $\text{RIPM} \rightarrow \text{RIPM}^T$ is only marginally better than the gradient flow observed while training $\text{PM} \rightarrow \text{PM}^T$. Then, why RIPM^T is better than PM^T ?

Comparison of the initial seed sparse networks' weight distribution shown in Fig. 4(a) demonstrates that the magnitude of active weights in RIPM is lower than that of PM. As we know, the poor gradient flows result in low magnitudes of newly activated parameters' weights after the thickening phase, and the magnitude of parameter weights of RIPM (i.e., initially active) are also low; allowing newly active parameters to be selected (and replace previously active ones) during the pruning step, leading to changes in the structure of sparse network during training. Such changes allow the model to learn new concepts, leading to higher performance in the obtained RIPM^T .

Thus, the parameter weights inherited from a fully converged dense network are responsible for $\text{PM} \rightarrow \text{PM}^T$'s inefficient learning at high sparsity amounts. This finding further motivates the effectiveness of training a verified locally robust sparse network from scratch rather than pruning an over-parameterized pre-trained dense model.

Error	PM	PM^T	RSM^T	$RIPM^T$
Standard	90.0	90.0	65.01	65.81
PGD	90.0	90.90	70.43	69.85
Verified	90.0	90.0	73.38	74.97

Table 3. Comparison for error metrics for sparse models obtained using different seed networks for a 4-layer CNN at 99% sparsity

Sparsity \Rightarrow Error	0%	80%	90%	95%	99%
Standard	4.04	4.42	4.38	5.52	11.55
PGD	9.35	11.60	10.10	13.84	17.22
Verified	14.23	11.85	10.75	13.90	18.70

Table 4. Error metrics for sparse models obtained using **SparseVLR** using LSTM trained for MNIST at various sparsity amounts

5.2 Application to Sequential Model

To further investigate the application of **SparseVLR** to sequential networks, we evaluated a small LSTM [56] as a backbone architecture to obtain sparse models for MNIST. Tab. 4 demonstrates the *standard*, *PGD*, and *verified* errors for the sparse models obtained using **SparseVLR**. It can be noted that up to 95% sparsity amount, the sparse models generalize comparable to their dense counterparts. Additionally, higher error at 99% sparsity can be attributed to the insufficient number of parameters for the target task.

5.3 Evaluations for Application-Relevant Datasets

Tab. 5 demonstrates the results for two application-relevant image datasets: (a) SVHN and (b) a pedestrian detection dataset that aims at differentiating between people and people-like objects [33]. The backbone architecture used for these evaluations is a 7-layer CNN, adapted to the respective datasets. For both SVHN and Pedestrian detection, the error metrics of the models having 99% sparsity are comparable to that of their dense counterparts. The perturbation amount used for SVHN and Pedestrian Detection are 8/255 and 2/255, respectively. Additionally, sparse models constructed for a sentiment analysis NLP dataset [30] on an LSTM model [22, 56] exhibit errors within 1% of the dense counterparts, showing **SparseVLR**’s generalizability (detailed results presented in Appendix F).

6 Design Choices for **SparseVLR**

• **Pruning after every thickening step:** Liu *et al.* [26] suggests that allowing the model to grow for multiple epochs before pruning results in exploring all the parameters at least once. However, the implicit sparsification caused by the $\mathcal{L}_{\text{train}}$ (discussed in Sec. 3) does not allow such exploration. Our empirical evaluations show that *pruning* step

Dataset Sparsity \Rightarrow Error	SVHN			Pedestrian Detection		
	0%	95%	99%	0%	95%	99%
Standard	62.55	62.77	65.87	28.40	26.22	28.40
PGD	68.19	68.23	70.52	42.35	39.66	43.03
Verified	74.87	75.21	76.76	63.53	67.39	63.02

Table 5. Error metrics for sparse models obtained using **SparseVLR** using 7 layer CNN as backbone architecture trained for (a) SVHN and (b) Pedestrian Detection at different sparsities

Dataset	Method \Rightarrow Error	IBP	CROWN	CROWN-Fast	CROWN-IBP
MNIST $\varepsilon = 0.4$	Standard	7.44	52.3	13.53	7.23
	PGD	10.27	68.84	18.20	9.68
	Verified	21.54	93.13	42.18	21.95
CIFAR $\varepsilon = 8/255$	Standard	62.85	69.04	68.72	65.01
	PGD	78.21	71.53	81.69	70.43
	Verified	78.52	88.3	89.39	73.38

Table 6. Error metrics for different formal verification mechanism used to compute $\mathcal{L}_{\text{train}}$ on 4 layer CNN trained for MNIST and CIFAR-10 at 99% sparsity

after every *thickening* step results in the most optimal sparse models.

• **Using CROWN-IBP as bounding mechanism:** Tab. 6 compares the errors exhibited by 4-layer CNN at 99% sparsity when trained by employing different bounding mechanisms to compute $\mathcal{L}_{\text{train}}$: IBP [14], CROWN [61], Fastened-CROWN [29], and CROWN-IBP [60]. Notably, empirically CROWN-IBP results in the most optimal models for both MNIST and CIFAR. Hence, **SparseVLR** employs CROWN-IBP to compute $\mathcal{L}_{\text{train}}$.

7 Discussion on Impact and Limitations

Impact: **SparseVLR** will enable resource-constraint platforms to leverage verified robust models. The sparse training reduces the total training time to almost half that of conventional pruning. Moreover, the inference time of the sparse models is *five times* lesser, on average, than their dense counterparts on NVIDIA RTX A6000 (detailed results presented in Appendix H).

Limitations and Future-works: • **SparseVLR** uses CROWN-IBP; thus, the results obtained are restricted by the robustness achieved by CROWN-IBP. Therefore, **SparseVLR** will need to be tailored for further advancement in verified local robustness training mechanisms. • Secondly, the empirical analysis has been done for models used in the literature [55, 60], and we show that sparse models exist for such architectures. However, further analysis of more complex networks and domains would be beneficial, which is out of the scope of this paper. • Finally, there is rich literature on pruning. However, we only investigated global

unstructured pruning mechanisms; since the focus was on training sparse models from scratch, and a rigorous investigation of pruning was out of the scope. •Our preliminary results on applying static-mask-based *sparse-training* paradigm based on ‘Lottery Ticket Hypothesis’ [7] for verified locally robust sparse NN search show inferior performance for this domain, suggesting the requirement for further investigation leveraging more sophisticated approaches for finding the *lottery ticket*. •Finally, following most studies in literature, this paper addresses up to 99% model sparsification. However, our analysis shows on extreme sparsity (99.9%), generalizability decrease, indicating optimal sparsity is between that range (99-99.9%). A detailed discussion is in Appendix G. Though finding optimal sparsity is out of scope, future work on this scope would be beneficial.

8 Conclusion

This is the first work investigating and showing that a verified locally robust sparse network is trainable from scratch, leveraging a dynamic-mask-based mechanism. The ability to train a sparse network from scratch renders the conventional requirement of training a dense network nonobligatory and reduces the training time to almost half. Additionally, the empirical analysis demonstrates *SparseVLR*’s generalizability, thus, enabling the deployment of verified locally robust models in resource-constrained safety-critical systems.

References

- [1] Ron Banner, Itay Hubara, Elad Hoffer, and Daniel Soudry. Scalable methods for 8-bit training of neural networks. In S. Bengio, H. Wallach, H. Larochelle, K. Grauman, N. Cesa-Bianchi, and R. Garnett, editors, *Advances in Neural Information Processing Systems*, volume 31. Curran Associates, Inc., 2018. 1, 13
- [2] Osbert Bastani, Yani Andrew Ioannou, Leonidas Lampropoulos, Dimitrios Vytiniotis, Aditya V. Nori, and Antonio Criminisi. Measuring neural net robustness with constraints. In *NIPS*, 2016. 12
- [3] Brian Chmiel, Liad Ben-Uri, Moran Shkolnik, Elad Hoffer, Ron Banner, and Daniel Soudry. Neural gradients are near-lognormal: improved quantized and sparse training. In *International Conference on Learning Representations*, 2021. 13
- [4] X. Dai, H. Yin, and N. K. Jha. Nest: A neural network synthesis tool based on a grow-and-prune paradigm. *IEEE Transactions on Computers*, 68(10):1487–1497, oct 2019. 1, 3, 4, 5, 13, 14
- [5] Thomas Elsken, Jan Hendrik Metzen, and Frank Hutter. Neural architecture search: A survey. *J. Mach. Learn. Res.*, 20(1):1997–2017, jan 2019. 13
- [6] Utku Evci, Yani Ioannou, Cem Keskin, and Yann Dauphin. Gradient flow in sparse neural networks and how lottery tickets win. *Proceedings of the AAAI Conference on Artificial Intelligence*, 36(6):6577–6586, Jun. 2022. 3, 4, 5, 7, 14, 15
- [7] Jonathan Frankle and Michael Carbin. The lottery ticket hypothesis: Finding sparse, trainable neural networks. In *International Conference on Learning Representations*, 2019. 3, 9, 13
- [8] Jonathan Frankle, Gintare Karolina Dziugaite, Daniel Roy, and Michael Carbin. Linear mode connectivity and the lottery ticket hypothesis. In *International Conference on Machine Learning*, pages 3259–3269. PMLR, 2020. 3, 13
- [9] Jonathan Frankle, Gintare Karolina Dziugaite, Daniel M. Roy, and Michael Carbin. Stabilizing the lottery ticket hypothesis, 2019. 3, 13
- [10] Aymeric Fromherz, Klas Leino, Matt Fredrikson, Bryan Parno, and Corina Pasareanu. Fast geometric projections for local robustness certification. In *International Conference on Learning Representations*, 2021. 2
- [11] Sayan Ghosh, Karthik Prasad, Xiaoliang Dai, Peizhao Zhang, Bichen Wu, Graham Cormode, and Peter Vajda. Pruning compact convnets for efficient inference, 2022. 3, 14
- [12] Yunchao Gong, L. Liu, Ming Yang, and Lubomir D. Bourdev. Compressing deep convolutional networks using vector quantization. *ArXiv*, abs/1412.6115, 2014. 13
- [13] Ian J. Goodfellow, Jonathon Shlens, and Christian Szegedy. Explaining and harnessing adversarial examples. *CoRR*, abs/1412.6572, 2015. 1
- [14] Sven Gowal, Krishnamurthy Dvijotham, Robert Stanforth, Rudy Bunel, Chongli Qin, Jonathan Uesato, Relja Arandjelovic, Timothy Mann, and Pushmeet Kohli. On the effectiveness of interval bound propagation for training verifiably robust models, 2018. 1, 2, 3, 5, 8, 12, 13
- [15] Song Han, Xingyu Liu, Huizi Mao, Jing Pu, Ardavan Pedram, Mark A. Horowitz, and William J. Dally. Eie: Efficient inference engine on compressed deep neural network, 2016. 3, 14
- [16] Song Han, Huizi Mao, and William J Dally. Deep compression: Compressing deep neural networks with pruning, trained quantization and huffman coding. *arXiv preprint arXiv:1510.00149*, 2015. 1, 3, 13, 14
- [17] Song Han, Jeff Pool, John Tran, and William J. Dally. Learning both weights and connections for efficient neural networks. In *Proceedings of the 28th International Conference on Neural Information Processing Systems - Volume 1*, NIPS’15, page 1135–1143, Cambridge, MA, USA, 2015. MIT Press. 1, 3, 13, 14
- [18] Geoffrey Hinton, Jeff Dean, and Oriol Vinyals. Distilling the knowledge in a neural network. pages 1–9, 03 2014. 13
- [19] Torsten Hoefler, Dan Alistarh, Tal Ben-Nun, Nikoli Dryden, and Alexandra Peste. Sparsity in deep learning: Pruning and growth for efficient inference and training in neural networks. *J. Mach. Learn. Res.*, 22(1), jan 2021. 3, 13, 14
- [20] Xiaowei Huang, Marta Kwiatkowska, Sen Wang, and Min Wu. Safety verification of deep neural networks. In Rupak Majumdar and Viktor Kunčak, editors, *Computer Aided*

Verification, pages 3–29, Cham, 2017. Springer International Publishing. 12

[21] Itay Hubara, Matthieu Courbariaux, Daniel Soudry, Ran El-Yaniv, and Yoshua Bengio. Quantized neural networks: Training neural networks with low precision weights and activations. *J. Mach. Learn. Res.*, 18(1):6869–6898, jan 2017. 13

[22] Robin Jia, Aditi Raghunathan, Kerem Göksel, and Percy Liang. Certified robustness to adversarial word substitutions, 2019. 8, 12

[23] Guy Katz, Clark Barrett, David L. Dill, Kyle Julian, and Mykel J. Kochenderfer. Reluplex: An efficient smt solver for verifying deep neural networks. In Rupak Majumdar and Viktor Kunčak, editors, *Computer Aided Verification*, pages 97–117. Springer International Publishing, 2017. 1, 12

[24] Byung-Kwan Lee, Junho Kim, and Yong Man Ro. Masking adversarial damage: Finding adversarial saliency for robust and sparse network. In *Proceedings of the IEEE/CVF Conference on Computer Vision and Pattern Recognition (CVPR)*, pages 15126–15136, June 2022. 1

[25] Hao Li, Asim Kadav, Igor Durdanovic, Hanan Samet, and Hans Peter Graf. Pruning filters for efficient convnets. *ArXiv*, abs/1608.08710, 2017. 1, 3, 13, 14

[26] Shiwei Liu, Lu Yin, Decebal Constantin Mocanu, and Mykola Pechenizkiy. Do we actually need dense over-parameterization? in-time over-parameterization in sparse training. In Marina Meila and Tong Zhang, editors, *Proceedings of the 38th International Conference on Machine Learning*, volume 139 of *Proceedings of Machine Learning Research*, pages 6989–7000. PMLR, 18–24 Jul 2021. 3, 5, 8, 13

[27] Zhuang Liu, Jianguo Li, Zhiqiang Shen, Gao Huang, Shoumeng Yan, and Changshui Zhang. Learning efficient convolutional networks through network slimming. *2017 IEEE International Conference on Computer Vision (ICCV)*, pages 2755–2763, 2017. 3, 5, 14

[28] Zhuang Liu, Mingjie Sun, Tinghui Zhou, Gao Huang, and Trevor Darrell. Rethinking the value of network pruning. In *International Conference on Learning Representations*, 2019. 3, 14

[29] Zhaoyang Lyu, Ching-Yun Ko, Zhifeng Kong, Ngai Wong, Dahua Lin, and Luca Daniel. Fastened crown: Tightened neural network robustness certificates. *ArXiv*, abs/1912.00574, 2020. 2, 5, 8

[30] Andrew L. Maas, Raymond E. Daly, Peter T. Pham, Dan Huang, Andrew Y. Ng, and Christopher Potts. Learning word vectors for sentiment analysis. In *Proceedings of the 49th Annual Meeting of the Association for Computational Linguistics: Human Language Technologies*, pages 142–150, Portland, Oregon, USA, June 2011. Association for Computational Linguistics. 2, 5, 8, 12

[31] Aleksander Madry, Aleksandar Makelov, Ludwig Schmidt, Dimitris Tsipras, and Adrian Vladu. Towards deep learning models resistant to adversarial attacks. In *International Conference on Learning Representations*, 2018. 1

[32] Eran Malach, Gilad Yehudai, Shai Shalev-Schwartz, and Ohad Shamir. Proving the lottery ticket hypothesis: Pruning is all you need. In Hal Daumé III and Aarti Singh, editors, *Proceedings of the 37th International Conference on Machine Learning*, volume 119 of *Proceedings of Machine Learning Research*, pages 6682–6691. PMLR, 13–18 Jul 2020. 3, 13

[33] Chandran Saravanan N J Karthika. Addressing false positives in pedestrian detection. In *International Conference on Electronic Systems and Intelligent Computing (ESIC 2020)*, 3 2020. 2, 5, 8, 12

[34] Adam Paszke, Sam Gross, Soumith Chintala, Gregory Chanan, Edward Yang, Zachary DeVito, Zeming Lin, Alban Desmaison, Luca Antiga, and Adam Lerer. Automatic differentiation in pytorch. 2017. 5

[35] Ana Pereira and Carsten Thomas. Challenges of machine learning applied to safety-critical cyber-physical systems. *Machine Learning and Knowledge Extraction*, 2(4):579–602, 2020. 1

[36] Luca Pulina and Armando Tacchella. Challenging smt solvers to verify neural networks. *AI Commun.*, 25(2):117–135, apr 2012. 12

[37] PyTorch. Pruning tutorial. <https://pytorch.org/tutorials/intermediate/pruning-tutorial.html#pruning-tutorial.3>

[38] Chongli Qin, James Martens, Sven Gowal, Dilip Krishnan, Krishnamurthy (Dj) Dvijotham, Alhussein Fawzi, Soham De, Robert Stanforth, and Pushmeet Kohli. *Adversarial Robustness through Local Linearization*. Curran Associates Inc., Red Hook, NY, USA, 2019. 1

[39] Tara N. Sainath, Brian Kingsbury, Vikas Sindhwani, Ebru Arisoy, and Bhuvana Ramabhadran. Low-rank matrix factorization for deep neural network training with high-dimensional output targets. In *2013 IEEE International Conference on Acoustics, Speech and Signal Processing*, pages 6655–6659, 2013. 1, 13

[40] Victor Sanh, Thomas Wolf, and Alexander M. Rush. Movement pruning: Adaptive sparsity by fine-tuning. In *NeurIPS*, 2020. 1, 3, 13, 14

[41] Victor Sanh, Thomas Wolf, and Alexander M. Rush. Movement pruning: Adaptive sparsity by fine-tuning, 2020. 3, 14

[42] Pedro Savarese, Hugo Silva, and Michael Maire. Winning the lottery with continuous sparsification, 2020. 3, 13

[43] Abigail See, Minh-Thang Luong, and Christopher D. Manning. Compression of neural machine translation models via pruning, 2016. 3, 14

[44] Vikash Sehwag, Shiqi Wang, Prateek Mittal, and Suman Jana. Towards compact and robust deep neural networks. *preprint arXiv:1906.06110*, 2019. 1, 3, 13, 14

[45] Vikash Sehwag, Shiqi Wang, Prateek Mittal, and Suman Jana. Hydra: Pruning adversarially robust neural networks. *34th Conference on Neural Information Processing Systems (NeurIPS 2020)*, 2020. 1, 3, 12, 13, 14

[46] Gagandeep Singh, Timon Gehr, Markus Püschel, and Martin Vechev. An abstract domain for certifying neural networks. *Proc. ACM Program. Lang.*, 3(POPL), jan 2019. 2

[47] Sidak Pal Singh and Dan Alistarh. Woodfisher: Efficient second-order approximation for neural network compression. In H. Larochelle, M. Ranzato, R. Hadsell, M.F. Balcan, and H. Lin, editors, *Advances in Neural Information*

Processing Systems, volume 33, pages 18098–18109. Curran Associates, Inc., 2020. 3, 14

[48] Aman Sinha, Hongseok Namkoong, and John Duchi. Certifiable distributional robustness with principled adversarial training. In *International Conference on Learning Representations*, 2018. 12

[49] Chong Min John Tan and Mehul Motani. DropNet: Reducing neural network complexity via iterative pruning. In Hal Daumé III and Aarti Singh, editors, *Proceedings of the 37th International Conference on Machine Learning*, volume 119 of *Proceedings of Machine Learning Research*, pages 9356–9366. PMLR, 13–18 Jul 2020. 3, 4, 13

[50] Vincent Tjeng, Kai Y. Xiao, and Russ Tedrake. Evaluating robustness of neural networks with mixed integer programming. In *International Conference on Learning Representations*, 2019. 1

[51] Shiqi Wang, Huan Zhang, Kaidi Xu, Xue Lin, Suman Jana, Cho-Jui Hsieh, and J Zico Kolter. Beta-CROWN: Efficient bound propagation with per-neuron split constraints for neural network robustness verification. In A. Beygelzimer, Y. Dauphin, P. Liang, and J. Wortman Vaughan, editors, *Advances in Neural Information Processing Systems*, 2021. 2

[52] Yisen Wang, Difan Zou, Jinfeng Yi, James Bailey, Xingjun Ma, and Quanquan Gu. Improving adversarial robustness requires revisiting misclassified examples. In *International Conference on Learning Representations*, 2020. 1

[53] Cody Marie Wild. Know your adversary: Understanding adversarial examples (part 1/2). <https://towardsdatascience.com/know-your-adversary-understanding-adversarial-examples-part-1-2-63af4c2f5830>. Published: 2018-01-23. 2

[54] Eric Wong and Zico Kolter. Provable defenses against adversarial examples via the convex outer adversarial polytope. In Jennifer Dy and Andreas Krause, editors, *Proceedings of the 35th International Conference on Machine Learning*, volume 80 of *Proceedings of Machine Learning Research*, pages 5286–5295. PMLR, 10–15 Jul 2018. 3, 5

[55] Eric Wong, Frank Schmidt, Jan Hendrik Metzen, and J. Zico Kolter. Scaling provable adversarial defenses. In S. Bengio, H. Wallach, H. Larochelle, K. Grauman, N. Cesa-Bianchi, and R. Garnett, editors, *Advances in Neural Information Processing Systems*, volume 31. Curran Associates, Inc., 2018. 3, 5, 6, 8, 12

[56] Kaidi Xu, Zhouxing Shi, Huan Zhang, Yihan Wang, Kai-Wei Chang, Minlie Huang, Bhavya Kailkhura, Xue Lin, and Cho-Jui Hsieh. Automatic perturbation analysis for scalable certified robustness and beyond. In *Proceedings of the 34th International Conference on Neural Information Processing Systems*, NIPS’20, Red Hook, NY, USA, 2020. Curran Associates Inc. 1, 2, 3, 5, 6, 8, 12, 13, 15

[57] Kaidi Xu, Huan Zhang, Shiqi Wang, Yihan Wang, Suman Jana, Xue Lin, and Cho-Jui Hsieh. Fast and complete: Enabling complete neural network verification with rapid and massively parallel incomplete verifiers. In *International Conference on Learning Representations*, 2021. 2

[58] Kaidi Xu, Huan Zhang, Shiqi Wang, Yihan Wang, Suman Jana, Xue Lin, and Cho-Jui Hsieh. Fast and complete: Enabling complete neural network verification with rapid and massively parallel incomplete verifiers. In *International Conference on Learning Representations*, 2021. 2

[59] Zhonghui You, Kun Yan, Jinmian Ye, Meng Ma, and Ping Wang. Gate decorator: Global filter pruning method for accelerating deep convolutional neural networks, 2019. 3, 13

[60] Huan Zhang, Hongge Chen, Chaowei Xiao, Sven Gowal, Robert Stanforth, Bo Li, Duane S. Boning, and Cho-Jui Hsieh. Towards stable and efficient training of verifiably robust neural networks. In *8th International Conference on Learning Representations, ICLR 2020, Addis Ababa, Ethiopia, April 26-30, 2020*. OpenReview.net, 2020. 1, 2, 3, 5, 6, 8, 12, 13, 14

[61] Huan Zhang, Tsui-Wei Weng, Pin-Yu Chen, Cho-Jui Hsieh, and Luca Daniel. Efficient neural network robustness certification with general activation functions. *ArXiv*, abs/1811.00866, 2018. 1, 2, 3, 5, 8, 13

[62] Jingfeng Zhang, Xilie Xu, Bo Han, Gang Niu, Lizhen Cui, Masashi Sugiyama, and Mohan Kankanhalli. Attacks which do not kill training make adversarial learning stronger. In Hal Daumé III and Aarti Singh, editors, *Proceedings of the 37th International Conference on Machine Learning*, volume 119 of *Proceedings of Machine Learning Research*, pages 11278–11287. PMLR, 13–18 Jul 2020. 1

[63] Tianyun Zhang, Shaokai Ye, Kaiqi Zhang, Jian Tang, Wu-jie Wen, Makan Fardad, and Yanzhi Wang. A systematic dnn weight pruning framework using alternating direction method of multipliers. In *Proceedings of the European Conference on Computer Vision (ECCV)*, pages 184–199, 2018. 1, 3, 13, 14

A Experiment Details

Datasets: The empirical analysis of **SparseVLR** is done for 5 datasets: MNIST, CIFAR, SVHN, Pedestrian Detection and Sentiment Analysis.

MNIST is a dataset of hand-written digits with 60000 samples in the training set and 10,000 samples in the testing set. All the images are in greyscale and have a size of 28×28 . The training set is generated using samples from approximately 250 writers. The writers for the test set and the training set are disjoint.

CIFAR-10 is a dataset of 60000 images evenly distributed among 10 mutually exclusive classes: airplanes, cars, birds, cats, deer, dogs, frogs, horses, ships, and trucks. The training set and the testing set consists of 50000 and 10000 images, respectively. These RGB images are of size 32×32 each. Additionally, The test set contains 1000 randomly selected images from each class, thus having a uniform distribution over all the classes.

SVHN is a real-world dataset for digit recognition. The images are Street View House Numbers obtained from google street view images. The format used for the evaluations for **SparseVLR** contains 32×32 images of individual digits with distractions. The dataset contains 73257 images in the training set and 26032 images for testing.

Pedestrian Detection [33] aims to differentiate between the person and person-like objects such as statues, scarecrows, etc., having very similar features to a person. The number of images in train, validate and test set are 944, 160, and 235, respectively, with a total of 1626 persons and 1368 non-human labeling.

SparseVLR is applicable to domains other than image classification. To illustrate this, an empirical study has been done on sentiment analysis NLP dataset [30] used in the previous formal verification approaches by [22, 56]. The dataset contains 10662 sentences evenly distributed between two classes: positive and negative.

Perturbation amount: For image classification datasets, the perturbations are introduced in ℓ_p -ball of radius ε (perturbation amount), $\mathbb{B}_p(x_0, \varepsilon)$ (defined in Sec. 2). The highest perturbation amounts (i.e., most difficult scenarios) used in the literature addressing formal verification and training [14, 55, 56, 60] are 0.4 and 8/255 for MNIST and CIFAR10, respectively. For CIFAR10, Zhang *et al.* [60] uses different perturbation amounts for training ($\varepsilon_{\text{train}}$) and testing ($\varepsilon_{\text{test}}$), such that $\varepsilon_{\text{train}} = 1.1 \times \varepsilon_{\text{test}}$, we follow the same convention. Thus, for the models that need to be tested for 8/255, the training is done for a perturbation amount of 8.8/255. For SVHN, the previous works targetting adversarial robustness [45], use perturbation amount of 8/255, thus, following the convention of CIFAR-10, we use $\varepsilon_{\text{test}} = 8/255$ and $\varepsilon_{\text{train}} = 8.8/255$. For Pedestrian Detection dataset, we use $\varepsilon_{\text{test}} = 2/255$ and

$$\varepsilon_{\text{train}} = 2.2/255.$$

For Sentiment analysis NLP dataset, the perturbations are introduced in terms of synonym-based word substitution in a sentence. Each word w has a set of synonyms $\mathbb{S}(w)$ with which it can be substituted. $\mathbb{S}(w)$ is computed using 8 nearest neighbors in counter-fitted word embedding, where the distance signifies similarity in meaning [22, 56]. The number of words being substituted is referred to as *budget* (δ). The maximum budget used in state-of-the-art [22, 56] for formal verification is 6, and we use the same amount.

Hyperparameters: The presented approach requires a set of hyperparameters as inputs: (T, s, l) , where T is the total number of training epochs, s is the epoch number at which the perturbation scheduler should start to increment the amount of perturbation and l specifies the length of the schedule, that is, the number of epochs in which the perturbation scheduler has to reach the maximum amount of perturbation ε_{max} .

These values are as follows: (1) For 4-layer CNN, 7-layer CNN, and Resnet, we use $(T, s, l) = (100, 10, 60)$ and $(T, s, l) = (2000, 200, 800)$, for MNIST and CIFAR-10, respectively; (2) For LSTM trained for MNIST, we use $(T, s, l) = (20, 1, 10)$; (3) For SVHN, the hyperparameters are same as that of CIFAR-10. (4) For Pedestrian Detection, the hyperparameters $(T, s, l) = (100, 20, 60)$ resulted in the models displaying the least errors empirically; and (5) For Sentiment Analysis NLP dataset, the hyperparameters $(T, s, l) = (25, 1, 10)$ are used. The value of (T, s, l) for MNIST, CIFAR-10, and Sentiment Analysis are in compliance with state-of-the-art [56]. For Pedestrian Detection and SVHN no prior hyperparameter values are available.

Learning rate: The training approach uses the learning rate scheduler, which gradually decreases the learning rate as the training proceeds after the maximum perturbation is reached. The starting learning is set to 10^{-4} as suggested by the state-of-the-art [56].

B Formal Verification

An NP-Complete problem: Linear Programming [2] and Satisfiability Modulo Theory (SMT) [20] have been used in literature as formal verification techniques to validate neural networks. However, Pulina and Tacchella [36] showed that Multi-Layer Perceptrons (MLPs) cannot be verified using SMT solvers, thus, challenging the scalability of SMT solvers to neural networks of realistic sizes. Furthermore, several applications require non-linear activation functions to learn complex decision boundaries, rendering the whole NN non-linear. The large size and non-linearity of NNs make the problem of formal robustness verification non-convex and NP-Complete [23, 48].

Relaxation based Methods: To address the challenges mentioned above, Katz *et al.* [23] used relaxation of ReLU

activations, temporarily violating the ReLU semantics, resulting in an efficient query solver for NNs with ReLU activations. The piece-wise linearity of the ReLU activations is the basis for this relaxation. LiRPA based methods such as CROWN [61], IBP [14], CROWN-IBP [60], etc. compute linear relaxation of a model containing general activation functions which are not necessarily piece-wise linear.

CROWN [61] uses a backward bounding mechanism to compute linear or quadratic relaxation of the activation functions. IBP [14] is a forward bounding mechanism that propagates the perturbations induced to the input towards the output layer in a forward pass based on interval arithmetic, resulting in ranges of values for each class in the output layer. CROWN-IBP [60] is a hybrid approach that demonstrated that IBP can produce loose bounds, and in order to achieve tighter bounds, it uses IBP [14] in the forward bounding pass and CROWN [61] in the backward bounding pass to compute bounding hyperplanes for the model. CROWN-IBP has been shown to compute tighter relaxations, thus, providing the most optimal results for formal verification.

As discussed in Sec. 2, the linear relaxation computed using LiRPA methods can be used to train verified locally robust models by minimizing L_{train} . This learning procedure uses a perturbation scheduler to gradually increase the amount of perturbation during training.

B.1 Perturbation Scheduler

ε -scheduler($\varepsilon_{\text{max}}, t, s, l$) aims to provide a perturbation amount for every training epoch $t \geq s$, which gradually increases ε starting at epoch s . The schedule starts with a 0 perturbation and reaches ε_{max} in l epochs [14]. Gowal *et al.* [14] proposed using ε -scheduler for training based on LiRPA and deems it necessary for an effective learning procedure. Since IBP [14] uses interval propagation arithmetic to propagate input perturbation to the output layer, where the interval size usually keeps on increasing as the propagations reach deeper in the model, the gradual increase of epsilon prevents the problem of intermediate bound explosion while training. Other related approaches also adopted the idea of gradual perturbation increment [56, 60]. Since the bounding mechanism used in **SparseVLR** is CROWN-IBP [60], the use of ε -scheduler is crucial.

C Model Compression

Several model compression approaches have been proposed to reduce the computational and storage requirements of deep neural networks (DNNs). Quantization aims to convert the parameter values to low-precision approximations requiring less storage bits per parameter [1, 3, 12, 21]. Model Distillation [18] and Neural Architecture Search [5]

train a smaller dense architecture that generalizes comparable to the dense network. Low-Rank Factorization [39] computes a matrix decomposition of the weight matrices, which requires fewer floating point operations. Model Sparsification/Pruning is the most common form of model compression, which constrains the model to use only a subset of original parameters for inference [16, 17, 25, 40, 44, 45, 63].

C.1 Model sparsification.

Hoefer *et al.* [19] categorizes the model sparsification according to the stage at which sparsification is performed: *train-and-sparsify* (After training), *sparsifying-during-training* (While Training) and *sparse-training* (Before training).

Train-and-sparsify approaches [16, 44, 45, 63] train a dense model and remove (or prune) the parameters contributing the least towards model inference. Since the removal of parameters may lead to loss of information learned by the original dense model, the removal of parameters is often followed by re-training the retained parameters, also known as the finetuning step. *Train-and-sparsify* associates a static binary mask with the parameters, which allows the finetuning step to update only the retained parameters.

The *sparsifying-during-training* mechanism gradually removes NN model parameters in small fractions per round. Each round is followed by a finetuning step allowing the model to recover from the parameter removal step [49, 59]. This is often called *iterative pruning*.

The *sparse-training* mechanism involves training a sparse network from scratch by using either a *static* or a *dynamic* mask. Identifying *static* masked sparse network is motivated by *Lottery Ticket Hypothesis (LTH)* [7] which states that “dense, randomly-initialized, feed-forward networks contain subnetworks (winning tickets) that - when trained in isolation - reach test accuracy comparable to the original network in a similar number of iterations”. However, finding the *static* mask in LTH [7–9, 32, 42] still requires a fully or partially trained dense model to start with.

Recently, *dynamic-mask-based sparse-training* mechanisms known as Dynamic Sparse Training (DST) have been developed. DST approaches [4, 26] start with a randomly initialized compressed sparse network and explore new network connections while learning network weights for the target task during training. **SparseVLR** adapts a DST approach to identify verified locally robust sparse network from scratch.

C.2 Selecting the parameters to be removed:

While all sparsification approaches mentioned above perform network parameters (i.e., weight) removal, selecting such parameter weights is done based on different crite-

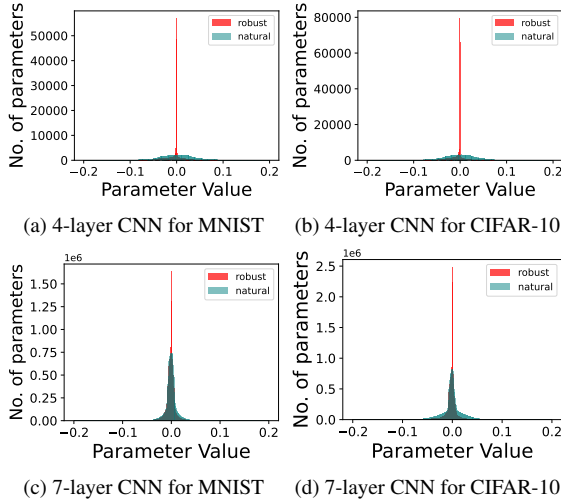


Figure 6. Weight distributions for (a) 4-layer CNN (MNIST) (b) 4-layer CNN (CIFAR-10) (c) 7-layer CNN (MNIST) (d) 7-layer CNN (CIFAR-10). The epsilon amounts used for robust training are 0.4 and 8.8/255 for MNIST and CIFAR-10, respectively.

ria such as the magnitude of weights, magnitude of corresponding gradients, minimal impact on Hessian matrix, etc. [19]. Magnitude-based pruning is the most popular pruning mechanism [15–17, 25, 40, 44, 45, 63], which removes the least magnitude parameters suggesting that the importance of a parameter is directly proportional to the magnitude of their weights.

Moreover, removal of parameters can be done either per-layer or globally, whereas recent studies [11, 27, 28, 43, 47] suggest the higher efficacy of global unstructured pruning. Sanh *et al.* [41] demonstrated that global magnitude-based pruning tends to prune earlier layers of a network by a lesser amount. Since the earlier layers for most networks are feature extraction layers which hold more importance for a classification task, it can be concluded that global pruning captures the importance of a layer as a whole.

D CROWN-IBP causes regularization

The motivation for **SparseVLR** is that a huge fraction of parameters of locally robust models trained using CROWN-IBP have low magnitudes, so removal of such less significant parameters has minimal effect on the model generalizability (Sec. 3).

Fig. 6 shows the weight distribution of models trained to minimize natural, and verified locally robust (CROWN-IBP [60]) losses. The trends are shown for 4-layer and 7-layer CNNs trained for MNIST and CIFAR-10 datasets. As evident from the distribution of weights, a higher fraction

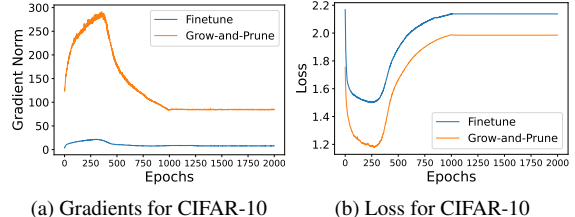


Figure 7. (a) Gradient flow and (b) loss during training a globally pruned 4-layer CNN using fine-tuning, and re-training using grow-and-prune CIFAR-10 datasets for perturbation of 0.4 and 8/255, respectively

of weights in verified locally robust models have very low magnitudes ($\approx 10^{-40}$). This observation suggests that models trained to minimize $\mathcal{L}_{\text{train}}$ (Eq. 4) penalize the parameter magnitudes.

E Explaining the generalizability difference for various sparse training mechanisms

E.1 Conventional Finetuning vs Grow-and-Prune

Conventional finetuning aiming to minimize $\mathcal{L}_{\text{train}}$ ((#ii) in Sec. 3) increases the *standard* and *verified* error even at small compression amounts. Such increment can be attributed to poor gradient flow encountered during static mask-based finetuning, which is in agreement with [6]. However, retraining a pruned model using *grow-and-prune* ((#iii) in Sec. 3) does not suffer from poor gradient flow, hence may help maintain the generalizability of the sparse compressed models.

To further investigate, Fig. 7 compares the losses and ℓ_1 -norm of gradients encountered while re-training a globally pruned network using conventional static mask-based finetuning (while keeping the mask the same throughout the training), and grow-and-prune mechanism [4]. The results are shown for a 4-layer CNN trained for CIFAR-10 at 90% sparsity. It is important to note that the training procedure uses ε -scheduling, which provides 0 perturbation for initial s epochs and then gradually increases the perturbation value. This results in an initial drop in losses, as seen in Fig. 7(b). As the perturbation amount increases, the loss increases as well and finally stabilizes.

Notably, the losses encountered by finetuning are higher than retraining using grow-and-prune, thus resulting in higher errors in the obtained compressed models (shown in Fig. 7(b)). The difference in losses encountered using the two approaches can be attributed to the difference in gradi-

ent flows (see Fig. 7(a)). Re-training using *grow-and-prune* incurs higher gradient flows than conventional finetuning, and according to Evci *et al.* [6], higher gradient flows lead to efficient training.

E.2 Training PM vs RSM

As discussed in Sec. 5, the effectiveness of **SparseVLR** is established by comparing the sparse models obtained by applying Algorithm 1 (steps 3-9) to different seed networks: PM (Pruned Model) and RSM (Random Sparse Model). Tab. 7 compares the sparse models obtained using three mechanisms: PM (Global Pruning), PM^T (Retaining PM using Algorithm 1 steps 3-9.) and RSM^T (obtained using **SparseVLR**). The results are shown for 3 backbone architectures: 4-layer CNN, 7-layer CNN and Resnet at 4 sparsity amounts: 80%, 90%, 95% and 99%; trained for two datasets MNIST and CIFAR-10. It can be noted that RSM^T outperforms both PM and PM^T especially at high sparsity amount such at 99%.

To investigate the difference in losses encountered while training $PM \rightarrow PM^T$ and $RSM \rightarrow RSM^T$ at 99% sparsity, Fig. 8 (same as Fig. 3) shows the difference in loss evolution for both the scenarios. It can be noted that $PM \rightarrow PM^T$ incurs higher loss than $RSM \rightarrow RSM^T$, thus resulting in higher errors.

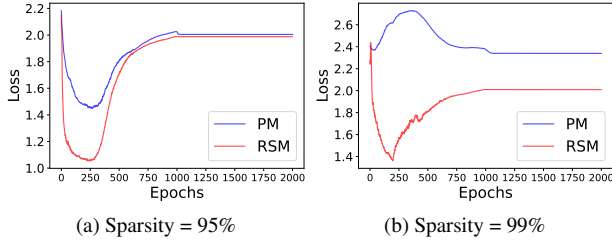


Figure 8. Variation of training loss for CIFAR-10 dataset on 4-layer CNN with $\epsilon_{\text{test}} = 8/255$ at two sparsity amounts (a) 95% and (b) 99%

Interestingly, at 99% sparsity, the loss evolution for $PM \rightarrow PM^T$ training does not follow the expected pattern, i.e. an initial decrease followed by an increase (see Fig. 8). The reason for this can be attributed to poor gradient flow while training $PM \rightarrow PM^T$ at 99% sparsity (as shown in Fig. 3(b) in Sec. 5). The low magnitude of gradient results in low magnitude in the newly activated parameters, which eventually get removed during the pruning step. On the other hand, the already active parameters, which are significantly high in magnitudes, tend to become more polarized, thus, resulting in over-fitting. However, with an initial high loss, the gradient flow increases enough to generate some newly activated parameters with sufficient magnitude

Sparsity \Rightarrow	0%	80%	90%	95%	99%
Standard	20.92	20.26	22.24	21.11	21.53
Verified	24.27	22.35	23.94	23.53	23.72

Table 8. Error metrics for sparse models obtained using our approach using LSTM as the backbone architecture trained for NLP dataset at different sparsity amounts

to replace the already activated parameters, which results in some decrease and eventually stabilization of the loss.

F Application to NLP for sentiment analysis

As discussed in Appendix A, for the Sentiment Analysis dataset, the perturbations are introduced in terms of synonym-based word substitution in a sentence, and the number of words substituted is called the *budget* δ . The value of δ used in the empirical analysis is 6.

Notably, this training does not use ℓ_p -norm perturbation, but to keep the perturbation amount continuous, the training procedure consists of an initial warm-up phase [56]. If the word at index i for a clean sentence and a perturbed sentence are represented by w_i and \hat{w}_i , and $e(w)$ is the embedding for the word w , the effective embedding used during training is given by:

$$e(w_i) = \epsilon * e(\hat{w}_i) + (1 - \epsilon) * e(w_i)$$

The value of ϵ is gradually increased from 0 to 1 during the training phase. The results thus produced for the original dense model (sparsity = 0%) are in compliance with state-of-the-art [56]. Table 8 shows that the sparse models obtained at different compression amounts using the presented approach exhibit *standard* and *verified* errors comparable to the original dense model. PGD attack is based on ℓ_p -norm perturbation which is not applicable to this domain, so the results shown in Table 8 does not include results for *PGD* error.

G Extreme sparsity:

The results presented in Tab. 2 show that the 99% sparse models generalize comparable to the dense model, thus, indicating the possibility of exploring further sparsity. However, at 99.9% sparsity the 7-layer CNN exhibit an increment of approximately 7% in *standard error* and 10% in *verified error* for both MNIST and CIFAR. This suggests that an optimal sparsity exists in the range of (99% - 99%) at which the sparse model generalizes comparable to its dense counterpart.

Dataset			MNIST					CIFAR-10				
Model	$\mathcal{M}_{\theta \downarrow}$ Type	Sparsity \Rightarrow Error	0% \mathcal{M}_{θ}	80%	90%	95%	99%	0%	80%	90%	95%	99%
4-layer CNN	PM	Standard	5.11	5.98	12.98	59.83		60.0	61.28	84.33	90.0	
		PGD	6.75	7.84	16.03	62.19		67.3	68.05	86.43	90.0	
		Verified	18.49	22.80	40.7	79.18		71.41	72.02	87.4	90.0	
	PM^T	Standard	5.29	4.78	4.79	4.78	6.97	59.88	58.81	59.32	60.73	90.0
		PGD	10.93	6.34	6.30	6.23	8.98	67.25	68.46	66.01	66.74	90.90
		Verified	18.07	17.71	17.22	17.46	21.35	71.5	70.86	71.04	72.12	90.0
	RSM^T	Standard	5.67	5.71	6.59	8.09		60.83	60.78	61.26	64.14	
		PGD	7.56	7.62	9.00	10.63		68.45	67.08	67.13	69.09	
		Verified	19.22	19.33	20.84	23.14		72.15	71.90	72.45	73.43	
7-layer CNN	PM	Standard	2.31	2.32	2.32	8.06		56.69	70.78	84.05	90.0	
		PGD	5.71	9.72	99.93	81.91		68.75	82.63	84.88	90.0	
		Verified	99.01	84.77	100.0	100.0		68.83	79.54	86.19	90.0	
	PM^T	Standard	2.27	1.85	2.05	3.37	2.11	56.08	54.59	55.33	55.24	90.0
		PGD	6.19	3.52	3.93	4.85	3.61	68.65	68.46	67.59	67.21	90.0
		Verified	12.2	12.25	11.96	14.51	12.06	68.66	68.5	68.49	69.6	90.0
	RSM^T	Standard	2.37	72.32	3.01	2.76		55.11	55.41	56.96	59.14	
		PGD	4.11	3.88	4.21	4.75		67.17	68.26	68.30	67.04	
		Verified	12.54	12.39	12.6	12.83		68.60	68.84	69.12	71.21	
Resnet	PM	Standard	3.68	6.51	4.09	62.06		55.68	88.06	90.0	90.0	
		PGD	6.03	8.98	5.74	64.36		65.24	89.41	90.0	90.0	
		Verified	16.62	20.97	19.34	82.02		70.41	89.44	90.0	90.0	
	PM^T	Standard	3.65	3.24	73.23	3.17	3.12	53.6	53.38	55.17	90.0	90.0
		PGD	9.11	4.22	4.16	4.04	3.98	63.83	64.37	66.25	90.0	90.0
		Verified	14.30	13.45	13.52	13.34	13.80	68.58	68.57	69.28	90.0	90.0
	RSM^T	Standard	3.54	3.91	3.88	4.95		55.36	56.30	57.99	60.31	
		PGD	4.53	5.05	5.16	6.77		66.55	67.44	67.04	68.88	
		Verified	15.5	15.06	15.39	17.74		68.95	69.33	70.14	71.38	

Table 7. Error Metrics for 4-layer CNN, 7-layer CNN, and Resnet trained for MNIST ($\varepsilon_{\text{train}} = 0.4$ and $\varepsilon_{\text{test}} = 0.4$) and CIFAR ($\varepsilon_{\text{train}} = 8.8/255$ and $\varepsilon_{\text{test}} = 8/255$) at different sparsity amounts

Compression \Rightarrow Model	0%	80%	90%	95%	99%
4 Layer CNN	1.8×10^{-5}	4.9×10^{-6}	5.2×10^{-6}	7.5×10^{-6}	6.4×10^{-6}
7 Layer CNN	1.1×10^{-4}	1.8×10^{-5}	1.8×10^{-5}	1.8×10^{-5}	1.7×10^{-5}
Resnet	1.1×10^{-4}	2.5×10^{-5}	2.5×10^{-5}	2.9×10^{-5}	2.8×10^{-5}

Table 9. Inference Time (in sec) at different sparsity amounts

H Computation time benefit

In addition to reduction of non-zero (active) parameters of a model, we observe that the the sparse models obtained using our approach incur much less computation time. We measure the computation time in terms of average inference time on NVIDIA RTX A6000 required per sample in a dataset. The computation time shown in Table 9 are computed for CIFAR-10 dataset for three models: 4 layer CNN, 7 layer CNN and Resnet at different sparsity amounts. It can be noted that the inference time required by the sparse models obtained using **SparseVLR** is on an average 5 times less than the inference time of the dense models.